IEEE Access
Multidisciplinary | Rapid Review | Open Access Journal

Received 5 July 2024, accepted 28 July 2024, date of publication 1 August 2024, date of current version 12 August 2024.

Digital Object Identifier 10.1109/ACCESS.2024.3436667

RESEARCH ARTICLE

Modified Fault Current Calculation Scheme Combined With MMC Control for AC/DC Distribution Networks

YUBO YUAN[1], JUAN LI[1], PENGPENG LYU[1], ZHONGHAO QIAN[2], YUNLONG JIANG[1], AND JIAMING WANG[1]

[1]Electric Power Research Institute, State Grid Jiangsu Electric Power Co., Ltd., Nanjing 210000, China
[2]Nantong Power Supply Branch, State Grid Jiangsu Electric Power Co., Ltd., Nantong 226001, China

Corresponding author: Juan Li (juanli0325@126.com)

This work was supported by the Science and Technology Project of State Grid Jiangsu Electric Power Company Ltd., under Grant J2023047.

ABSTRACT The existing fault current analysis in distribution networks tend to ignore the impact of the control dynamics arising from AC/DC converters. In response to the abovementioned challenge, this paper introduces a novel fault current estimation calculation approach tailored for AC/DC distribution networks, specifically considering the control dynamics of Modular Multilevel Converters (MMC). The methodology commences with the simplified model of the AC/DC distribution networks. Subsequently, on the basis of the analysis for the control structure of MMC, the impact of various control dynamics on fault current is quantified. Then, the branch currents and node voltages are obtained through a set of voltage-current differential equations. To validate the proposed method, simulation verification is conducted using PSCAD/EMTDC. The calculation results of main branch currents demonstrate that the accuracy of the improved method is about 90%, which shows the effectiveness of the proposed method. Furthermore, the robustness of the presented method against the variations of voltage level, breaker delay, and transition resistance is validated, where its accuracy is over 80%.

INDEX TERMS AC/DC distribution networks, control dynamics, different grid conditions, fault current estimation calculation, MMC.

NOMENCLATURE

PARAMETERS

C_{SM}	Capacitor of each sub-module.
R_{arm}	Resistance on each arm.
L_{arm}	Inductance on each arm.
N_{SM}	Number of sub-modules in each arm.
C_c	Equivalent capacitor.
L_c	Equivalent inductor.
R_c	Total equivalent resistor.
R_{on}	Resistance to the activated IGBT.
i_s	Source current.
u_c	Capacitor voltage.
i_c	Capacitor current.
u_{dc}	DC voltage.
P^*	AC control power.
Q^*	Reactive power control power.
U_{dc}^*	DC control voltage.
k_p	Proportional gain of voltage control.
k_i	Integral gain of voltage control.
D_{dc}	Droop control parameter.
k_{pp}	Proportional gain of power and voltage droop control.
k_{pi}	Integral gain of power and voltage droop control.
R_{dc}	An equivalent resistor of the overhead line.
L_{dc}	An equivalent inductor of the overhead line.
S1	The gate signal of IGBT1.
S2	The gate signal of IGBT2.
R_0	Fault resistance.
P_{nom}	Nominal power in voltage control.

The associate editor coordinating the review of this manuscript and approving it for publication was Arturo Conde.

© 2024 The Authors. This work is licensed under a Creative Commons Attribution-NonCommercial-NoDerivatives 4.0 License.
For more information, see https://creativecommons.org/licenses/by-nc-nd/4.0/

U_{nom}	Nominal voltage in voltage control.
Z_{ij}	Sum of the line impedance from node$i$ to node j.
i_{ij}	Branch current from node i to node j.
u_i	Node voltage of node i.
R_{ij}	Sum of the line resistance from node$i$ to node j.
L_{ij}	Sum of the line inductance from node$i$ to node j.
R_{ci}	Total equivalent resistor of MMC in node i.
L_{ci}	Equivalent inductor of MMC in node i.
C_i	Equivalent capacitor of MMC in node i.
R_{mer}	Errors rate between simulated and calculated values.
S_i	Calculated value.
S_i^*	Simulated value.
N	The number of sampling points.

ABBREVIATIONS

MMC	Modular multilevel converters.
AC	Alternating current.
DC	Direct current.
VSC	Voltage source converter.
HVDC	High voltage direct current.
RLC	Resistor, inductor and capacitor.
SM	Sub-module.
IGBT	Insulated gate bipolar transistor.
AVM	Average value model.
PV	Power and voltage.
PI	Proportions and integrals.
PQ	Active power and reactive power control mode.
VQ	Voltage and reactive power control mode.
RL	Resistor and inductor.
MER	Mean error rate.

SETS

R	Equivalent resistance matrix.
L	Equivalent inductance matrix.
C	Equivalent capacitance matrix.
A	Correlation matrix.
u	Node voltage matrix.
i	Branch current matrix.
R_t	Matrix constructed by resistance and inductance.
L_t	Matrix constructed by resistance and inductance.
K	Matrix about capacitor.

I. INTRODUCTION

With the continuous development of smart grids [1], AC/DC hybrid distribution networks will become the main structure of China's distribution network in the coming time [2]. For the sake of enhancing the controllability of distribution lines and reducing the probability of power accidents and accidental losses, multi-terminal joint power supply networks have been popularized and applied for power supply reliability [3]. At the same time, to reduce unnecessary costs, it is necessary to carry out the estimation calculation of fault currents in distribution lines. Besides, it is essential to get the fault currents for the purpose of determining the location and action design of circuit breakers before the protection design [4], [5], [6].

Numerous experts and scholars have devoted themselves to the estimation calculation of fault currents in electrical networks. Yang et al. derived simple numerical expressions for the fault currents in the DC circuit of a two-level voltage source converter (VSC), and the method was based on resonant circuit analysis for estimating the capacitive discharge current [7]. Cwikowski et al. analyzed the equivalent model of circuit faults for VSC in high voltage direct current (HVDC) networks [8]. With the increasing complexity of the distribution networks, VSC can no longer meet the demand, and MMC becomes a widely used structure. The MMC mechanism was analyzed and the line fault current was discussed from different perspectives in [9], [10], [11], [12], and [13]. Tang et al. divided the MMC into different approximate models by the distance from the line where the fault occurred, and took the external electrical characteristics of the MMC as the primary factor for fault current analysis [9]; Luo et al. considered the different discharges of each submodule in each arm of the MMC after the fault, and equated the internal MMC into different capacitors for fault current discussion [10]; Xing et al. investigated the basic fault current in AC side, and studied the two-terminal scenario from the MMC composition mechanism and fault discharge composition [11]. Although the MMC mechanism was analyzed comprehensively, the influence of control dynamic on fault current is discussed few. A generalized DC pole-to-pole short-circuit fault current estimation scheme was presented [14]. However, the article does not consider the influence of MMC, i.e., it lacks a discussion of the dynamic effects from the terminal controller. Langwasser et al. proposed an MMC equivalent model, but only analyzed the fault estimation of monopolar-bipolar high-voltage DC transmission lines [15]. Moreover, the above-mentioned study neglects the impact of grid condition variations on the reliability of estimation method. Fault current estimation for distributed generation units is provided in [16], [17], [18], and [19]. Liu et al. established a full-process state-space fault current calculation for wind farms [16], Mu et al. investigated a fault transient calculation considering the dynamics of the phase-locked loop structure in photovoltaic power [17], and Xu et al. developed an estimation of current sensor faults on the inverter side [18]. It is noteworthy that these studies address mostly a single branch in specific scenario. It means that these methods have high accuracy only at faulty branch.

Based on the above discussions, one should address the following points from the perspective of theoretical and practical value:

1) The existing schemes do not provide a method to get fault currents and node voltages simultaneously considering the control dynamics for MMC-based AC/DC distribution networks.
2) The existing schemes based on simplified models possess high descriptive accuracy only at faulty lines, which is defective for real-world applications.

3) The existing schemes do not take the variation of electrical network conditions into account so that the robustness will be limited for the complex topology.

To overcome the abovementioned issues, a novel fault current estimation calculation approach tailored for AC/DC distribution networks considering the control dynamics of MMC is developed in this study. The main contribution of this paper can be recited as follows:

1) This paper adopts the modified fault current estimation strategy considering the control dynamics of MMC, which provides a general methodology to get fault currents and node voltages in an MMC-based AC/DC distribution network.
2) The currents in branches that have no fault can be calculated correctly, which reveals a remarkable advantage in protection setting to avoid maloperation.
3) This study compares the simulation value with the calculated value under diverse electrical network conditions, which shows the great potential and practicality of the developed strategy.

The rest of the paper is organized as follows. The AC/DC distribution network including modified fault equivalent models of MMC and isolated loads is given in Section II. In Section III, the novel current calculation approach concerning MMC control is given. In Section IV, the simulation comparison under different grid situations is built to demonstrate the superior applicability of the proposed method. Section V concludes the paper.

Remark 1: With the continuous development of distribution networks, AC distribution networks are gradually being replaced by hybrid AC/DC distribution networks. Therefore, efforts have been made to calculate the line fault current before the protection design stage in the case of grid-connected complex converter equipment. However, the existing studies suffer from the following shortcomings: 1) the methodology is limited to HVDC transmission lines; 2) the control dynamics are insufficiently described; 3) the verification sections rarely discuss the impact of the grid voltage level and the load-breaker delay on the estimation algorithm. Based on the above analysis, this paper proposes a fault current calculation method considering MMC control dynamics. Compared with the results of the literature [15], for the first time, the fault equivalent model considering the control dynamics is combined with the AC/DC distribution network containing isolated loads, which expands the application scenario of this MMC fault equivalent model, and enriches the equivalent representation of source currents associated with the control dynamics. In addition, the comparative analysis has been carried out under various conditions such as different fault resistances, different voltage levels, and different circuit breaker delays, which is more convincing than simply changing the monopolar and bipolar structures from the perspective of real-world applications.

II. AC/DC DISTRIBUTION NETWORKS

A. MMC FAULT EQUIVALENT MODEL

The three-phase structure of the MMC is displayed in Fig. 1. Each phase is made up of upper and lower bridge arms, and every bridge arm consists of submodules (SMs) connected in series, each of which is a half-bridge structure including insulated gate bipolar transistors (IGBTs) and anti-parallel diodes. The shunt capacitor is C_{SM}, and the equivalent resistance and inductance on each arm are written as R_{arm} and L_{arm}.

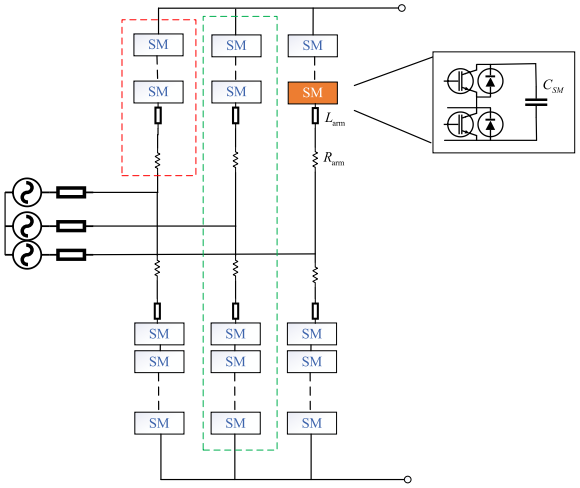

FIGURE 1. Circuit diagram of MMC.

This paper selects the modified model derived from average value theory, termed average value model (AVM), displayed in Fig. 2., to represent the MMC. i_s is the capacitor current. u_{dc} is the DC voltage. The DC side of MMC is approximated using RLC-equivalent circuits associated with current sources that are restrained [20], in which there exists an assumption that the converter has no losses, i.e., the AC power can be transmitted into the DC side completely.

Using the detailed model parameters [21], the equivalent capacitance C_c can be formulated as

$$C_c = \frac{6C_{SM}}{N_{SM}} \tag{1}$$

where C_{SM} and N_{SM} represents the capacitance and number of sub-modules (SMs) in each arm. Based on the circuit analysis, the equivalent inductance L_c can be further obtained as follows

$$L_c = \frac{2L_{\text{arm}}}{3} \tag{2}$$

Then, one can get the total equivalent resistance of the MMC [22]:

$$R_c = \frac{2(R_{\text{arm}} + \sum R_{on})}{3} \tag{3}$$

where R_{arm} and L_{arm} represent the values of resistance and inductance on each arm, and $\sum R_{on}$ represents all resistance for the activated IGBT. By modeling the IGBT blocking state

with a diode instead of an ideal switch, the modified AVM brings a huge enhancement to the DC current estimation.

Remark 2: The RLC equivalent model of MMC is usually used to analyze its dynamic characteristics and design the control strategy. The RLC equivalent model consists of the following parts:

1) Capacitance:

There is a capacitor in each sub-module for energy storage and output voltage smoothing. The total equivalent capacitance of all sub-module capacitors can be viewed as one large capacitor.

2) Resistance:

The equivalent resistance of the circuit elements in the submodule, such as switching tubes and capacitors. This equivalent resistance reflects the loss characteristics of the converter.

3) Inductance:

Due to the presence of inductive components (such as filter inductors and commutator inductors) in the converter, the system will exhibit a certain reactance characteristic.

Combining the above parts, the RLC equivalent circuit of MMC typically consists of an equivalent capacitance, an equivalent resistance, and an equivalent inductance in series.

In order to simplify the calculation, the average value model (AVM) is used to obtain the corresponding component parameters. Its rationality is mainly reflected in the following aspects:

1) Simplification of complexity:

MMC has a large number of submodules, and directly simulating the switching behaviors of all submodules is very complex and computationally huge. The AVM greatly simplifies the computational complexity by equivalent processing of each sub-module, making it possible to simulate and analyze large-scale systems.

2) Capturing key dynamic characteristics:

Although the AVM simplifies the specific switching behavior, it can effectively capture the key dynamic characteristics, such as current and voltage trends, which is very useful for designing control strategies.

3) Ease of control design:

Based on the AVM, designing and verifying control strategies is easier. The AVM provides a smoother system response, which helps in the tuning of controller parameters and performance optimization.

In summary, the AVM have important application values in power system analysis and control design. The reasonableness of the AVM is mainly reflected in the simplification of the analysis process of the complex system, and at the same time, it can accurately reflect the dynamic characteristics, which is convenient for the design and optimization of the control strategy.

The total control scheme of the MMC includes outer voltage control and inner current control. The simplified control diagram is displayed in Fig. 3. In general, the outer control mainly includes power control (P), voltage control (V) and

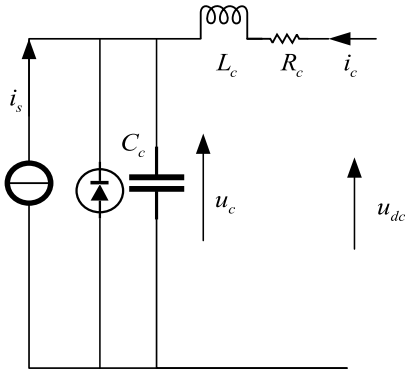

FIGURE 2. The diagram of AVM for MMC.

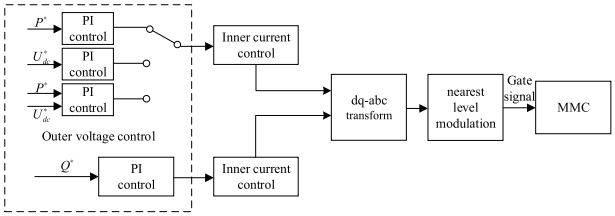

FIGURE 3. Simplified control diagram of the MMC.

power voltage droop control (PV droop). Considering that fault current estimation process only requires the knowledge of the input-output relationships for MMC, the outer control is mainly studied.

When the converter uses power control, the source current i_s can be obtained

$$i_s = \frac{P^*}{u_c} \tag{4}$$

where P^* is the AC control power and u_c is the capacitor voltage.

When the converter uses voltage control, the source current can be obtained from the voltage control loop as follows.

$$i_s = k_p(U_{dc}^* - u_c) + k_i \int (U_{dc}^* - u_c)dt \tag{5}$$

where U_{dc}^* is the DC control voltage, and k_p and k_i represent the proportional gain and integral gain, respectively.

When the converter uses power and voltage droop control, the source current can be obtained from the control loop as follows.

$$i_s = \frac{P^* + [k_{pp}(U_{dc}^* - u_c) + k_{pi}\int (U_{dc}^* - u_c)dt]D_{dc}}{u_c} \tag{6}$$

where D_{dc} is the droop control parameter, and k_{pp} and k_{pi} represent the proportional gain and integral gain, respectively. Besides, the reactive power control (Q) is also represented in Fig.3.

B. THE AC/DC DISTRIBUTION NETWORK WITH ISOLATED LOADS

In this paper, a four-terminal topology is adopted, and the AC/DC distribution network containing isolated loads with

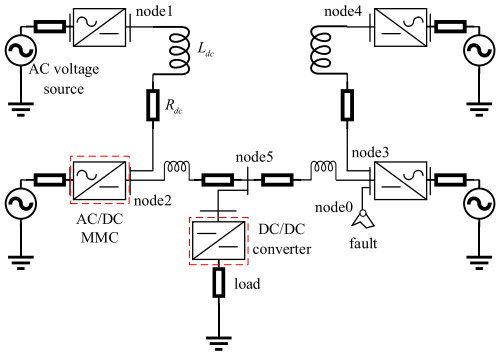

FIGURE 4. Four-terminal AC/DC distribution network.

DC/DC converter is taken as the research object. The specific topology is shown in Fig. 4. Each section of the overhead line is replaced by an equivalent RL model.

To effectively inhibit the rapid discharge of the capacitor on the high-voltage side of the DC/DC converter when a short-circuit fault occurs in the main line, two switching tubes in opposite directions are connected in series in the high-voltage side capacitance circuit [23], shown in Fig. 5. Associated with a short-circuit fault in the DC line, the controlled IGBT gate signals S1 and S2 are disconnected, and the circuit breaker of the DC/DC input port immediately starts to act. Through the cooperation of S1 and S2 with the circuit breaker, it can quickly cut off the capacitance circuit and effectively prevent the charging and discharging of the capacitor, thus ensuring that the fault current will be decreased to zero. Therefore, it will not have an impact on the fault current estimation accuracy.

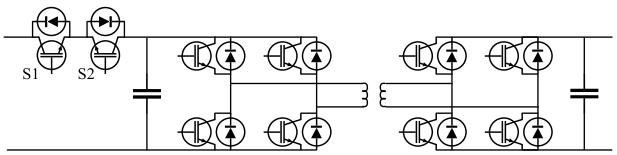

FIGURE 5. DC/DC converter.

III. FAULT CURRENT ESTIMATION CONSIDERING CONTROL DYNAMICS

Using the improved AVM of MMC and the equivalent RL model of the overhead line, this paper proposes a current estimation calculation scheme based on coupled differential equations for the pole-to-pole fault in AC/DC distribution networks. The pole-to-pole fault is set at node 0, and the AC/DC distribution network displayed in Fig. 4 can be simplified into an equivalent circuit model in Fig. 6. $i_s = [i_{s1}\ i_{s2}\ i_{s3}\ i_{s4}]^T$ denotes the source current vector which is determined by MMC control, R_0 is the fault resistance, $R = [R_{c1}\ R_{c2}\ R_{c3}\ R_{c4}]^T$ and $L = [L_{c1}\ L_{c2}\ L_{c3}\ L_{c4}]^T$ represent the equivalent resistance and inductance for MMC, and $C = [C_1\ C_2\ C_3\ C_4]^T$ is the equivalent capacitance. The equivalent resistance and inductance of each overhead transmission line is expressed in the form of Z. Z_{ij} denotes the sum of the line impedance from node i to node j. i_{ij} denotes the line current from node i to node j. u_i denotes the voltage of node i. R_0 denotes the fault resistance.

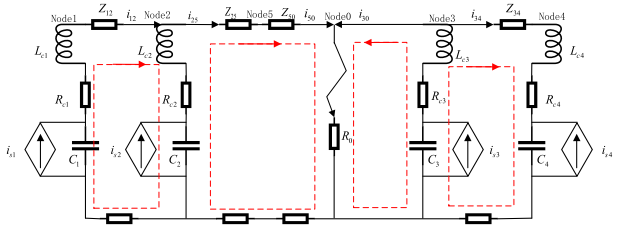

FIGURE 6. Equivalent model of pole-to-pole fault circuits.

As shown in Fig.6, the system is decoupled into four independent loops. Using Kirchhoff's voltage law, the four independent loops are expressed as following:

$$u_1 - u_2 = (2R_{12} + R_{c1})i_{12} + (2L_{12} + L_{c1})\frac{di_{12}}{dt} + R_{c2}(i_{12} - i_{25}) + L_{c2}\frac{d(i_{12} - i_{25})}{dt} \tag{7}$$

$$u_2 = R_{c2}(i_{25} - i_{12}) + L_{c2}\frac{d(i_{25} - i_{12})}{dt} + 2R_{25}i_{25} + 2L_{25}\frac{di_{25}}{dt} + 2R_{50}i_{50} + 2L_{50}\frac{di_{50}}{dt} + R_0(i_{30} + i_{50}) \tag{8}$$

$$u_3 = (i_{30} + i_{34})R_{c3} + L_{c3}\frac{d(i_{30} + i_{34})}{dt} + (i_{30} + i_{50})R_0 \tag{9}$$

$$u_3 - u_4 = R_{c3}(i_{30} + i_{34}) + L_{c3}\frac{d(i_{30} + i_{34})}{dt} + (2R_{34} + R_{c4})i_{34} + (2L_{34} + L_{c4})\frac{di_{34}}{dt} \tag{10}$$

Since the fault occurred at node 0 near node 3, the corresponding line impedance should be changed, i.e., $L_{50} = L_{53}$. Furthermore, node 5 is a node disconnecting with MMC, so $i_{25} = i_{50}$. Then the differential equations of each node can be established [14], and the dynamics of the branch current are given below

$$Au = R_t i + L_t\frac{di}{dt} \tag{11}$$

where A is the correlation matrix, R_t and L_t represent the matrix constructed by resistance and inductance. u and i represent the node voltage and the branch current, respectively. The element of A is determined based on the node voltage with respect to the branch in which it is located. When the node voltage vector is $u = [u_1\ u_2\ u_3\ u_4]^T$, the branch current vector is $i = [i_{12}\ i_{25}\ i_{30}\ i_{34}\ i_{50}]^T$. At this time the correlation matrix is

$$A = \begin{bmatrix} 1 & -1 & 0 & 0 \\ 0 & 1 & 0 & 0 \\ 0 & 0 & 1 & 0 \\ 0 & 0 & 1 & -1 \\ 0 & 0 & 0 & 0 \end{bmatrix} \tag{12}$$

It is noteworthy that the last row of the correlation matrix corresponds to all zero elements. Because there exists node 5 which is not in direct contact with MMC converters. It is impossible to write the differential equations directly from the RLC loop for node 5, and node 5 can only be indirectly obtained from the other nodes' differential equations.

The diagonal elements of R_t and L_t contain all the resistors and inductors on the branch current path. The diagonal elements of the branch ij are $2R_{ij} + R_{ci} + R_{cj}$ and $2L_{ij} + L_{ci} + L_{cj}$ respectively. The non-diagonal elements indicate the elements in the path through which the other branch currents flow. The symbols of the non-diagonal elements indicate the reference direction of the branch currents. Since the fault location is directly connected to node 3, the resistance and inductance matrices are collected as follows (13) and (14), as shown at the bottom of the page.

The MMC current vector $i_c = [i_{c1} \cdots i_{ci}]^T$ can be obtained from the branch currents

$$i_c = -A^T i \tag{15}$$

Therefore, in the fault current estimation, it is possible to consider the effect of source currents coming from different control strategies [15]. Assuming no losses in converters, u_c can then be approximated as the node voltage u. Based on Kirchhoff's current law and the relationship between the voltage u_c and current i_c, one can obtain

$$\frac{du_c}{dt} = K(i_c + i_s) \tag{16}$$

where $K = diag[\frac{1}{C_1} \cdots \frac{1}{C_i}]$, that is

$$K = \begin{bmatrix} \frac{1}{C_1} & 0 & 0 & 0 \\ 0 & \frac{1}{C_2} & 0 & 0 \\ 0 & 0 & \frac{1}{C_3} & 0 \\ 0 & 0 & 0 & \frac{1}{C_4} \end{bmatrix} \tag{17}$$

and i_s is the source current, which is calculated according to (4), (5), or (6). In power control, a constant source current is obtained, i.e., $\frac{di_s}{dt} = 0$. In voltage control, the source current derivative is obtained as

$$\frac{di_s}{dt} = \frac{P_{nom}}{U_{nom}^2}[k_i(U_{dc}^* - u_c) - k_p \frac{du_c}{dt}] \tag{18}$$

where P_{nom} and U_{nom} represent the nominal power and voltage for MMC. When the MMC uses power and voltage droop control, the ratio of D_{dc} and u_c is too small because k_{pp} is close to 0. Therefore, i_s mainly consists of the reference power of the MMC, and the contribution of the corresponding station for i_s can be approximated as a constant value, i.e., $\frac{di_s}{dt} = 0$. It is necessary to add (18) to the coupled differential equations, as shown in (11), and the spatiotemporal correlation of the source currents has to be added to the voltage differential equations to achieve the aim of considering the influence of the control dynamics in the current estimation.

Further, the following set of coupled differential equations can be obtained

$$\begin{aligned} u_1 - u_2 &= (2R_{12} + R_{c1} + R_{c2})i_{12} - R_{c2}i_{25} \\ &\quad + (2L_{12} + L_{c1} + L_{c2})\frac{di_{12}}{dt} - L_{c2}\frac{di_{25}}{dt} \end{aligned} \tag{19}$$

$$\begin{aligned} u_2 &= -R_{c2}i_{12} + (2R_{25} + R_{c2})i_{25} + R_0 i_{30} \\ &\quad + (R_0 + 2R_{53})i_{50} \\ &\quad - L_{c2}\frac{di_{12}}{dt} + (2L_{25} + L_{c2})\frac{di_{25}}{dt} + 2L_{53}\frac{di_{50}}{dt} \end{aligned} \tag{20}$$

$$\begin{aligned} u_3 &= (R_0 + R_{c3})i_{30} + R_{c3}i_{34} + R_0 i_{50} + L_{c3}\frac{di_{30}}{dt} \\ &\quad + L_{c3}\frac{di_{34}}{dt} \end{aligned} \tag{21}$$

$$\begin{aligned} u_3 - u_4 &= R_{c3}i_{30} + (2R_{34} + R_{c3} + R_{c4})i_{34} \\ &\quad + L_{c3}\frac{di_{30}}{dt} + (2L_{34} + L_{c3} + L_{c4})\frac{di_{34}}{dt} \end{aligned} \tag{22}$$

$$0 = i_{50} - i_{25} + \frac{di_{50}}{dt} - \frac{di_{25}}{dt} \tag{23}$$

$$\frac{du_1}{dt} = \frac{1}{C_1}(-i_{12} + i_{s1}) \tag{24}$$

$$\frac{du_2}{dt} = \frac{1}{C_2}(i_{12} - i_{25} + i_{s2}) \tag{25}$$

$$\frac{du_3}{dt} = \frac{1}{C_3}(-i_{30} - i_{34} + i_{s3}) \tag{26}$$

$$\frac{du_4}{dt} = \frac{1}{C_4}(i_{34} + i_{s4}) \tag{27}$$

For the convenience of the solution, the obtained coupled differential equation is reduced to the first-order differential form, which can obtain the node voltage and branch current. Owing to the fact that the obtained multivariate

$$R_t = \begin{bmatrix} 2R_{12} + R_{c1} + R_{c2} & -R_{c2} & 0 & 0 & 0 \\ -R_{c2} & 2R_{25} + R_{c2} & R_0 & 0 & R_0 + 2R_{53} \\ 0 & 0 & R_0 + R_{c3} & R_{c3} & R_0 \\ 0 & 0 & R_{c3} & 2R_{34} + R_{c3} + R_{c4} & 0 \\ 0 & -1 & 0 & 0 & 1 \end{bmatrix} \tag{13}$$

$$L_t = \begin{bmatrix} 2L_{12} + L_{c1} + L_{c2} & -L_{c2} & 0 & 0 & 0 \\ -L_{c2} & 2L_{25} + L_{c2} & 0 & 0 & 2L_{53} \\ 0 & 0 & L_{c3} & L_{c3} & 0 \\ 0 & 0 & L_{c3} & 2L_{34} + L_{c3} + L_{c4} & 0 \\ 0 & -1 & 0 & 0 & 1 \end{bmatrix} \tag{14}$$

differential equations does not have an analytical solution, we can improve the approximate accuracy of the numerical solution by bringing in the fault transient data of the distribution network.

$$\frac{di_{12}}{dt} = \frac{u_2 - u_1 - R_{c2}i_{25} + (2R_{12} + R_{c1} + R_{c2})i_{12} - L_{c2}\frac{di_{25}}{dt}}{-(2L_{12} + L_{c1} + L_{c2})} \tag{28}$$

$$\frac{di_{25}}{dt} = \frac{\begin{aligned}&\{L_{c2}u_2 - L_{c2}u_1 + L_{c2}(2R_{12} + R_{c1} + R_{c2})i_{12} - R_{c2}L_{c2}i_{25} \\ &+ (2L_{12} + L_{c1} + L_{c2})[-u_2 - R_{c2}i_{12} + R_0 i_{30} + \\ &(2R_{25} + R_{c2} + 2L_{53})i_{25} + (R_0 + 2R_{53} - 2L_{53})i_{50}]\}\end{aligned}}{L_{c2}^2 - (2L_{25} + L_{c2} + 2L_{53})(2L_{12} + L_{c1} + L_{c2})} \tag{29}$$

$$\frac{di_{30}}{dt} = \frac{u_3}{L_{c3}} + \frac{u_4}{2L_{34} + L_{c4}} - \left(\frac{R_0 + R_{c3}}{L_{c3}} + \frac{R_0}{2L_{34} + L_{c4}}\right)i_{30} + \left(\frac{2R_{34} + R_{c4}}{2L_{34} + L_{c4}} - \frac{R_{c3}}{L_{c3}}\right)i_{34} - \left(\frac{R_0}{L_{c3}} + \frac{R_0}{2L_{34} + L_{c4}}\right)i_{50} \tag{30}$$

$$\frac{di_{34}}{dt} = \frac{-u_4 + R_0 i_{30} - (2R_{34} + R_{c4})i_{34} + R_0 i_{50}}{2L_{34} + L_{c4}} \tag{31}$$

$$\frac{di_{50}}{dt} = \frac{di_{25}}{dt} \tag{32}$$

$$\frac{du_1}{dt} = \frac{1}{C_1}(-i_{12} + i_{s1}) \tag{33}$$

$$\frac{du_2}{dt} = \frac{1}{C_2}(i_{12} - i_{25} + i_{s2}) \tag{34}$$

$$\frac{du_3}{dt} = \frac{1}{C_3}(-i_{30} - i_{34} + i_{s3}) \tag{35}$$

$$\frac{du_4}{dt} = \frac{1}{C_4}(i_{34} + i_{s4}) \tag{36}$$

The diagram of the fault current calculation scheme is displayed in Fig. 7.

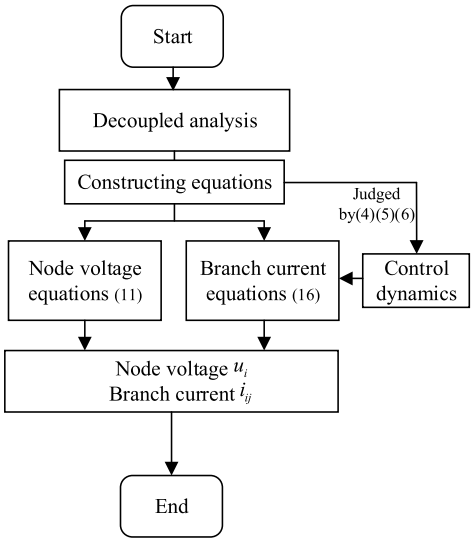

FIGURE 7. The diagram of fault current calculation scheme.

IV. VALIDATIONS

A four-terminal AC/DC distribution network is constructed in PSCAD/EMTDC to verify the correctness of fault current estimation, and the improved fault equivalent model of MMC used in this paper is compared with the MMC model without considering the control dynamics. The simulation parameters of the AC/DC grid are shown in Table 1. MMC parameters are shown in Table 2, where 'PQ' means active power and reactive power control, and 'VQ' means voltage and reactive power control.

TABLE 1. Parameters of AC/DC grid.

Parameters	Value
DC bus voltage	±10 kV
Fault transition resistance	0.01 Ω
Rated power	2 MW
Rated AC voltage at the primary side	10 kV
Rated AC voltage at the secondary side	11 kV
Equivalent resistance	0.006 Ω/km
Equivalent inductance	0.001 H/km

MW = megawatt, Ω = ohm, kV = kilovolt, km = kilometer, H = henry.

TABLE 2. Parameters of MMC.

Node	Equivalent inductance	Equivalent resistance	Number of sub-modules	Equivalent capacitance	Control mode	Reference
1	0.02H	0.18Ω	200	0.3mF	PQ	1MW
2	0.013H	0.12Ω	200	0.45mF	PQ	-2MW
3	0.02H	0.18Ω	200	0.03mF	VQ	20kV
4	0.0077H	0.73Ω	200	0.075mF	PQ	1MW

mF =microfarad.

Since the developed fault current estimation strategy is solved by the oscillating circuit equations, the calculated values are only taken for the first ten milliseconds after the fault occurs in order to keep the validity of estimation strategy.

Fig. 8 gives the comparison of the pole-to-pole fault currents of AC/DC distribution networks, where 'Imp' means the improved method, 'Tra' means the traditional AVM model without considering control dynamics, and 'Sim' represents the circuit simulation results. It can be found that the

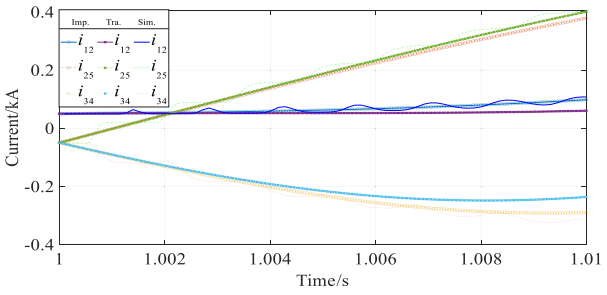

FIGURE 8. Comparison of pole-to-pole fault currents in AC/DC distribution networks.

developed method considering the MMC control dynamics exhibits superior results, which are closer to the simulation results than those by using the traditional equivalent approach, for the branch that are not contact directly with the faulted branch. In Fig.8, the fault transition resistance is 0.01 Ω. It is noteworthy that when the fault transition resistance is rather small, the branch current in the faulted branch will increase rapidly, which seems losing control. Thus, the proposed method shows no much better than the traditional approach in the faulted branch.

In order to give the detailed quantitative analysis, the mean error rate (MER) R_{mer} is used as following

$$R_{mer} = \frac{1}{N}\sum_{i=1}^{N}\left|\frac{S_i^* - S_i}{S_i^*}\right| \tag{37}$$

where S_i is the calculated value, S_i^* is the simulation value, and N is the number of total sampling points.

The MER in 10ms after the fault occurred are collected in Table 3. The difference in MER between the two methods is small in the faulty branch, but in the other branches where faults do not occur directly, the proposed method possesses the enhancement tremendously. Taking the branch current i_{12} as an example, the MER of the proposed method is reduced by more than 50% against the traditional method. In addition, the average MER of the improved method currents is less than 0.126, while the traditional method's average MER is over 0.17.

TABLE 3. The MER of different methods.

Method	i_{12}	i_{25}	i_{34}
Tra	0.1881	0.1778	0.1463
Imp	0.0846	0.2054	0.0807

To confirm the validity of the fault current estimation in distribution networks under different conditions, a comparison between calculated and simulated values is carried out for different voltage levels, load circuit breaker delays, and fault transition resistances. Fig. 9 shows the comparison results when the voltage of the original medium-voltage distribution networks is increased to 400 kV. We can see that branch currents using the improved method are closer to the simulated

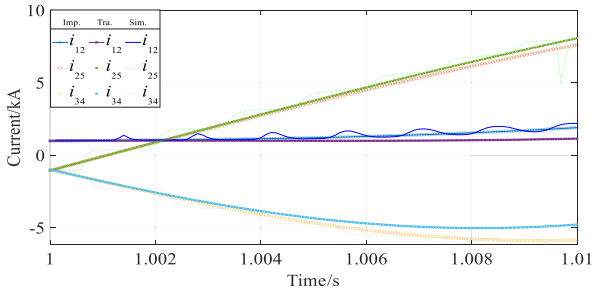

FIGURE 9. Comparison results between calculated values and simulation results with 400kV.

TABLE 4. The MER of different methods with the voltage level of 400KV.

Method	i_{12}	i_{25}	i_{34}
Tra	0.1859	0.2537	0.1205
Imp	0.0789	0.2730	0.0793

values than the traditional approach. The MER of different methods are shown in Table 4. The MER of the improved method also is less than the traditional one. Therefore, we can conclude that the developed scheme can still maintain the fault estimation accuracy under different voltage level grids.

The load can be isolated through the reverse series diode and circuit breaker to avoid the impact on the current estimation. However, the common circuit breaker is not yet able to respond rapidly, so the response time delay for the actual circuit breaker should be considered. In this paper, the response time delay is set as 10ms. Fig. 10 shows the comparison between the calculated values and the simulated values with the response time delay of the circuit breaker. The MER of different methods are shown in Table 5. It can be found that the developed fault current estimation scheme still has sufficient estimation accuracy against the traditional method.

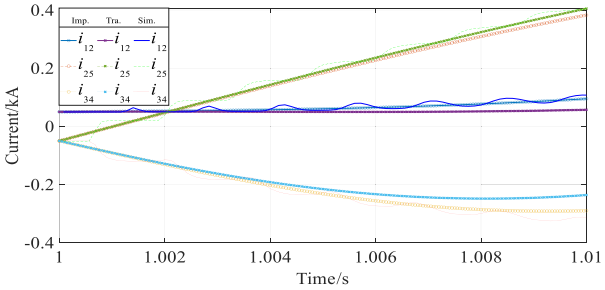

FIGURE 10. Comparison between the calculated values and simulation results when circuit breaker delay exists.

TABLE 5. The MER of different methods under breaker delay.

Method	i_{12}	i_{25}	i_{34}
Tra	0.2109	0.1683	0.1463
Imp	0.0820	0.1951	0.0807

When a non-metallic fault occurs, the fault resistance is usually relatively high. Therefore, we also need to verify the effectiveness of the proposed estimation strategy under fault resistance variation. Fig. 11 shows the comparison results under faulty transition resistance variation. The considered faulty transition resistance is 10Ω in Fig. 11. It can be found that this improved method is also able to estimate the line current with a certain robustness under different transition resistances. Table 6 demonstrates the MER of different methods. The MER of the improved method are totally lower than the traditional method.

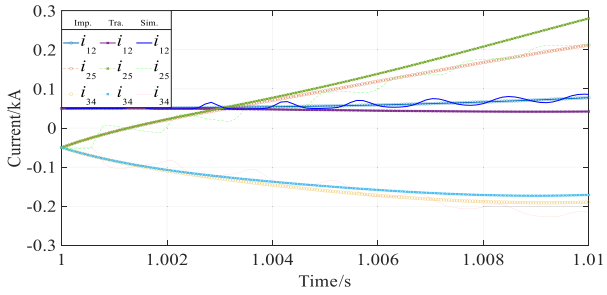

FIGURE 11. Comparison of calculated values and simulated values when transition resistance changes.

TABLE 6. The MER of different methods with the transition resistance of 10Ω.

Method	i_{12}	i_{25}	i_{34}
Tra	0.2085	0.4741	0.1215
Imp	0.0824	0.3757	0.1007

Remark 3: Line faults not only cause sharp changes in the current and voltage of the faulty line but also impact neighboring non-faulty lines through electrical coupling. To ensure the stable operation of the distribution network, it is crucial to estimate these current variations in advance, enabling the implementation of necessary protective measures. Understanding the current behavior of non-faulty lines under fault conditions can help optimize the settings of protective devices, thereby avoiding the maloperation of the protection equipment for non-faulty branches.

V. CONCLUSION

In this paper, a fault current estimation method is proposed, which takes the control dynamics of MMC in AC/DC distribution networks into consideration. On the basis of isolated DC loads and the improved equivalent models of MMC, a simplified circuit diagram is given. Besides, a chain of equations is gained. This paper achieves the accurate calculation of each DC branch current using coupled differential equations. From the quantitative analysis of different methods, it is easy to say that the modified model used in this scheme can maintain about 90% accuracy in different branch currents which is much better than the traditional model. Even in the different grid situations, the improved method still outperforms the traditional one. In voltage level of 400kV, the improved method shows better performance than the traditional one. Under the breaker delay, the traditional method could only keep 80% accuracy in calculating the currents on the far branches while the improved method keeps over 88% accuracy in each branch. When the transition resistance is increased, the mean error rates of traditional method are totally over the improved method. Compared with simulation, this estimation method reduces the time expense by calculating each DC branch current of the distribution network, which is beneficial in the design stage of grid protection. In the future, we can refine this method by taking more different situations into account, such as sophisticated electrical networks with a large number of distribution generations, high impedance fault, and timing fault.

REFERENCES

[1] X. Ding, Y. Zhang, and Z. Ye, "Current sensors offset fault online estimation in permanent magnet synchronous generator (PMSG) drives for offshore wind turbines," *IEEE Access*, vol. 9, pp. 135996–136003, 2021.

[2] D. Tzelepis, V. Psaras, E. Tsotsopoulou, S. Mirsaeidi, A. Dysko, Q. Hong, X. Dong, S. M. Blair, V. C. Nikolaidis, V. Papaspiliotopoulos, G. Fusiek, G. M. Burt, P. Niewczas, and C. D. Booth, "Voltage and current measuring technologies for high voltage direct current supergrids: A technology review identifying the options for protection, fault location and automation applications," *IEEE Access*, vol. 8, pp. 203398–203428, 2020.

[3] Y. Luo, J. He, M. Li, D. Zhang, Y. Zhang, Y. Song, and M. Nie, "Analytical calculation of transient short-circuit currents for MMC-based MTDC grids," *IEEE Trans. Ind. Electron.*, vol. 69, no. 7, pp. 7500–7511, Jul. 2022.

[4] K. Gajula, L. K. Marepalli, X. Yao, and L. Herrera, "Recursive least squares and adaptive Kalman filter-based state and parameter estimation for series arc fault detection on DC microgrids," *IEEE J. Emerg. Sel. Topics Power Electron.*, vol. 10, no. 4, pp. 4715–4724, Aug. 2022.

[5] Y. Sun, J. Yang, and Z. Zhang, "Single-loop robust decoupling control base on perturbation estimation for DC-based DFIG," *IEEE Access*, vol. 12, pp. 29759–29767, 2024.

[6] R. Aljarrah, M. Al-Omary, D. Alshabi, Q. Salem, S. Alnaser, D. Cetenovic, and M. Karimi, "Application of artificial neural network-based tool for short circuit currents estimation in power systems with high penetration of power electronics-based renewables," *IEEE Access*, vol. 11, pp. 20051–20062, 2023.

[7] J. Yang, J. E. Fletcher, and J. O'Reilly, "Short-circuit and ground fault analyses and location in VSC-based DC network cables," *IEEE Trans. Ind. Electron.*, vol. 59, no. 10, pp. 3827–3837, Oct. 2012.

[8] O. Cwikowski, B. Chang, M. Barnes, R. Shuttleworth, and A. Beddard, "Fault current testing envelopes for VSC HVDC circuit breakers," in *Proc. 11th IET Int. Conf. AC DC Power Transmiss.*, Birmingham, U.K., Feb. 2015, pp. 1–8.

[9] S. Tang, G. Jia, and C. Zhang, "A calculation method of analytical DC fault current in MMC-HVDC grid including current-limiting devices," in *Proc. IEEE Energy Convers. Congr. Exposit. (ECCE)*, Detroit, MI, USA, 2020, pp. 5276–5282.

[10] G. Luo, X. Zhang, Y. Liu, D. Li, Y. He, and L. Yang, "Fault current calculation of MMC-HVDC with varying capacitance equivalents," in *Proc. IEEE Sustain. Power Energy Conf. (iSPEC)*, Chengdu, China, Nov. 2020, pp. 1754–1759.

[11] F. Xing, Y. Liu, Z. Li, J. Xu, W. Cheng, and X. Song, "Analysis and calculation of symmetrical ground fault short circuit current contributed by MMC-HVDC converter station at AC side," in *Proc. IEEE 4th Int. Conf. Renew. Energy Power Eng. (REPE)*, Beijing, China, Oct. 2021, pp. 163–167.

[12] M. M. F. Darwish, M. H. A. Hassan, N. M. K. Abdel-Gawad, and D. A. Mansour, "Application of infrared spectroscopy for discrimination between electrical and thermal faults in transformer oil," in *Proc. 9th Int. Conf. Condition Monitor. Diagnosis (CMD)*, Kitakyushu, Japan, Nov. 2022, pp. 255–258.

[13] M. M. F. Darwish, M. H. A. Hassan, N. M. K. Abdel-Gawad, and D. A. Mansour, "A new method for estimating transformer health index based on ultraviolet-visible spectroscopy," in *Proc. 23rd Int. Middle East Power Syst. Conf. (MEPCON)*, Cairo, Egypt, Dec. 2022, pp. 1–5.

[14] C. Li, C. Zhao, J. Xu, Y. Ji, F. Zhang, and T. An, "A pole-to-pole short-circuit fault current calculation method for DC grids," *IEEE Trans. Power Syst.*, vol. 32, no. 6, pp. 4943–4953, Nov. 2017.

[15] M. Langwasser, G. De Carne, M. Liserre, and M. Biskoping, "Fault current estimation in multi-terminal HVdc grids considering MMC control," *IEEE Trans. Power Syst.*, vol. 34, no. 3, pp. 2179–2189, May 2019.

[16] X. Liu, Z. Zhang, Y. Liu, Z. Liu, M. Su, C. Li, L. Ge, X. Zhang, and P. Wang, "Fault current unified calculation method for whole process fault ride-through of DFIG-based wind farms," *IEEE Trans. Smart Grid*, vol. 15, no. 1, pp. 485–503, Jan. 2023.

[17] R. Mu, J. He, B. Li, W. Wang, C. Yao, and Y. Zhang, "Transient fault current calculation method of photovoltaic grid-connected system considering the dynamic response of phase-locked loop," in *Proc. IEEE/IAS Ind. Commercial Power Syst. Asia (ICPS Asia)*, Chongqing, China, Jul. 2023, pp. 1292–1297.
[18] S. Xu, Z. Zheng, W. Huang, Y. Liu, and H. Chen, "Current sensor fault estimation and fault tolerance of grid-connected three-level NPC inverter based on reduced-order observer," in *Proc. 6th Int. Conf. Robot., Control Autom. Eng. (RCAE)*, Suzhou, China, Nov. 2023, pp. 234–238.
[19] M. M. F. Darwish, M. H. A. Hassan, N. M. K. Abdel-Gawad, M. Lehtonen, and D. A. Mansour, "A new technique for fault diagnosis in transformer insulating oil based on infrared spectroscopy measurements," *High Voltage*, vol. 9, no. 2, pp. 319–335, Apr. 2024.
[20] R. Vidal-Albalate and J. Forner, "Modeling and enhanced control of hybrid full Bridge–Half bridge MMCs for HVDC grid studies," *Energies*, vol. 13, no. 1, p. 180, Jan. 2020.
[21] J. Hu, K. Xu, L. Lin, and R. Zeng, "Analysis and enhanced control of Hybrid-MMC-Based HVDC systems during asymmetrical DC voltage faults," *IEEE Trans. Power Del.*, vol. 32, no. 3, pp. 1394–1403, Jun. 2017.
[22] H. Jia, J. Yin, T. Wei, Q. Huo, J. Li, and L. Wu, "Short-circuit fault current calculation method for the multi-terminal DC grid considering the DC circuit breaker," *Energies*, vol. 13, no. 6, p. 1347, Mar. 2020.
[23] S. Behzadirafi and F. de León, "Closed-form determination of the impedance locus plot of fault current limiters: Asymmetrical faults," *IEEE Trans. Power Del.*, vol. 35, no. 2, pp. 754–762, Apr. 2020.

YUBO YUAN received the Ph.D. degree in electrical engineering from Southeast University, Nanjing, China, in 2016. He is currently a Senior Researcher-Level Engineer with State Grid Jiangsu Electric Power Company Ltd., China. His research interests include power system relay protection, DC transmission, and distribution control.

JUAN LI received the Ph.D. degree in electrical engineering from Shandong University, Jinan, China, in 2016. She is currently an Engineer with State Grid Jiangsu Electric Power Company Ltd., China. Her current research interest includes protection of distributed networks.

PENGPENG LYU received the Ph.D. degree in electrical engineering from Hohai University, China, in 2018. She is currently a Senior Engineer with State Grid Jiangsu Electric Power Company Ltd., China. Her research interests include distribution networks, load data, power systems, and active distribution networks.

ZHONGHAO QIAN received the B.S. and Ph.D. degrees in electrical engineering from Xi'an Jiaotong University, China, in 2010 and 2016, respectively. He is currently an Engineer with State Grid Jiangsu Electric Power Company Ltd., China. His research interests include distribution dispatching, the simulation study of vacuum arc, and intelligent control.

YUNLONG JIANG received the B.S. degree in power electronics and power transmission from State Grid Electric Power Research Institute, China, in 2016. He is currently an Engineer with State Grid Jiangsu Electric Power Company Ltd., China. His research interests include power electronics, power supply reliability calculation analysis, and short-term prediction.

JIAMING WANG received the M.S. degree in electrical engineering from Zhejiang University, Hangzhou, China, in 2021. He is currently an Engineer with State Grid Jiangsu Electric Power Company, Ltd., China. His research interests include base classifiers, classification framework, and identification of disturbances.